NEXRES 3 (2026) 101120

Contents lists available at ScienceDirect

Next Research

journal homepage: www.elsevier.com/locate/nexres

Investigation of the impact of atmospheric conditions on the catalytic conversion of phenolic vapor via copper-loaded zeolite-Y catalyst

Lasanga Amarasena [a,b], Rohan Weerasooriya [a], Athula Bandara [c], Xing Chen [d], Lakmal Jayarathna [a,*]

[a] National Institute of Fundamental Studies, Hanthana Road, Kandy 20000, Sri Lanka
[b] Postgraduate Institute of Science, University of Peradeniya, Peradeniya 20400, Sri Lanka
[c] Department of Chemistry, Faculty of Science, University of Peradeniya, Peradeniya 20400, Sri Lanka
[d] Institute of Industry and Equipment Technology, Hefei University of Technology, Hefei 230009, China

ARTICLE INFO

Keywords:
Catalytic conversion
Hydrothermal synthesis
Phenol vapor
Reaction conditions
Zeolite CuY catalyst

ABSTRACT

This study explores the catalytic degradation of phenol vapor using a copper-loaded zeolite Y (CuY) catalyst synthesized via a hydrothermal (HT) seed-assisted method. Comprehensive characterization confirmed that the HT-Zeolite CuY catalyst exhibits an enhanced morphology and increased availability of active copper cations, which were successfully incorporated into specific aluminum sites within the zeolite supercage. Phenol degradation was investigated under various atmospheric conditions, including inert environments, the presence of oxygen and moisture, and the addition of hydrogen peroxide (H_2O_2). Reaction products were analyzed using gas chromatography-mass spectrometry (GC/MS) to elucidate degradation pathways. Under inert conditions, partial phenol conversion was observed with 60.17 % phenol removal, suggesting the in-situ generation of reactive oxygen species (ROS) on the catalyst surface, consistent with a Fenton-like mechanism. The main degradation products included ethanol, 2-butanone, 2-pentanone, and p-benzoquinone. The introduction of oxygen accelerated degradation, while moderate humidity improved initial conversion. However, excessive moisture inhibited catalytic activity, likely due to competitive adsorption or pore blockage. In the presence of H_2O_2, complete phenol degradation was achieved, yielding formic acid, methylal, acetic acid, and methyl acetate as major products. These results demonstrate that the HT-Zeolite CuY catalyst is highly effective for phenol vapor conversion across a range of conditions, highlighting the catalytic role of surface-bound copper in facilitating oxidative degradation. The findings underscore the potential of this material for environmental remediation applications involving volatile organic compounds (VOCs) and support the relevance of Fenton-like mechanisms in dry and humid oxidation systems.

1. Introduction

Phenol emissions arise from diverse anthropogenic and natural sources. Industrial sectors such as petrochemicals, textiles, pesticides, and phenolic resin production are the primary contributors, along with emissions from combustion processes, paints, and waste incineration [1]. Domestic emissions are mainly due to the use of cleaning solutions and wood burning; they are also found in plastics and cigarette smoke [2,3]. Volatilization from ambient water and soils is a natural outdoor source of phenol emission; however, because it is a slow process, the effect is minimal [1]. Higher levels of phenol in the air can be expected in urban areas, mainly due to traffic emissions via vehicle exhaust and waste gas emissions near industrial zones.

Due to the health risk of phenol vapor inhalation, which is in increased concentrations, remediation of Phenolic Volatile Organic Compounds (VOC) has become an important necessity [4]. Phenol is an extremely potent odor that can be detected at a threshold of 0.04 ppm [5]. Once phenols enter the air, they typically degrade within 1–2 days through mechanisms such as photodegradation and oxidation by hydroxyl radicals or nitrogen oxides (NO_x) [4]. Furthermore, phenol can interact with other pollutants, leading to the formation of harmful secondary pollutants, such as photochemical smog [4,10–12]. The World

* Corresponding author.
E-mail addresses: lrlasanga@gmail.com (L. Amarasena), rohan.we@nifs.ac.lk (R. Weerasooriya), athulatbandara@yahoo.com (A. Bandara), xingchen@hfut.edu.cn (X. Chen), lakmal.ja@nifs.ac.lk (L. Jayarathna).

https://doi.org/10.1016/j.nexres.2025.101120
Received 26 August 2025; Received in revised form 17 November 2025; Accepted 18 November 2025
Available online 19 November 2025

Health Organization (WHO) has reported that exposure to phenol, whether through contact or inhalation, can cause irritation and burns to the skin, eyes, and respiratory tract. Prolonged exposure may lead to organ damage and systemic poisoning [11]. The World Health Organization (WHO) has highlighted the lack of comprehensive data regarding atmospheric phenol concentrations. According to their reported data, background levels should be below 1 ng m^{-3}, while urban and suburban areas exhibit higher levels, ranging from 0.1 to 8 μg m^{-3}. In industrial zones, phenol concentrations can reach values up to two orders of magnitude greater. However, reported occupational exposure levels should not exceed 19 mg m^{-3} [11]. Moreover, employers must adhere to OSHA's (2005a) regulations, which require them to minimize exposure to phenol at or below eight hours and a time-weighted average (TWA) of 5 ppm by implementing engineering and work practice controls [6]. ACGIH (2005) and NIOSH (2005) also suggest an occupational exposure limit of 5 ppm TWA [6].

Several methods are used to remediate phenolic vapor in industrial and environmental contexts, each leveraging unique mechanisms to reduce toxicity and environmental impact. Despite extensive research on the aqueous degradation of phenol, comparatively fewer studies address its removal in the gas phase [7–12]. Among those, most gas-phase studies have been conducted utilizing computational calculations. For example, there is a study by C. Xu and L. Wang [11], has investigated the gas-phase oxidation mechanism of phenol using DFT and ab initio calculations [11]. However, there are some other studies conducted under laboratory conditions. G. Moussavi and M. Mohseni et al [7], have investigated the biodegradation of phenol-contaminated air streams in bio trickling filters, packed with polyurethane foam cubes and enriched with phenol-degrading mixed culture [7]. The removal efficiency of phenol in this study was only 57 % and they concluded that it depends on the inlet concentration and flow rate [7]. Moreover, C. Lai et al [9], and F. Arena et al [10], have studied Catalytic wet air oxidation (CWAO) of phenol.

Catalytic oxidation is widely regarded as an efficient, eco-friendly, and cost-effective method for converting VOCs into less harmful substances such as carbon dioxide and water [13,14]. This study focuses on utilizing catalytic oxidation for the removal of phenolic compounds. The phenol degrades into various degradation products in its oxidizing pathway, and a cationic catalyst can accelerate the reaction. When phenol partially degrades in the presence of a metal cation catalyst and oxygen, various intermediate products are formed. In contrast, if it undergoes complete oxidation or mineralization, carbon dioxide and water are the final products. There have been used different types of catalysts for phenol degradation, such as cation or metal oxide catalysts [9, 15–19], photocatalysts [20–23], catalysts with electrochemical [24], etc. However, cationic catalytic reactions can be considered a highly effective method for the degradation of phenol, offering a more convenient method than other techniques such as photocatalysis and ozonation, as these methods often involve substantial costs and energy expenditures, underscoring the advantages of utilizing cationic catalysis in this context [25]. Most of the studies on phenol degradation have been done by focusing on wastewater remediation with the advanced oxidation process (AOP) [15,26–30]. But the use of costly oxidants (H_2O_2, $KMnO_4$, O_3, UV-irradiation, etc [16]) limits the feasibility of advanced oxidation processes (AOP) to small-scale applications [10]. However, no definitive pathway has been established for this degradation mechanism.

Conventional homogeneous catalysts used for phenol oxidation processes include mineral acids, simple metal ions, and metal complexes. However, these catalysts are difficult to extract from the reaction mixture. Therefore, researchers have been exploring heterogeneous catalysis using various cations, metal oxides, and complexes, such as supported or pure metal oxides, metal complex oxides, zeolite-encapsulated metal complexes, and hydrotalcite-like compounds [31]. Support material for the catalyst can either be inert or actively participate in the catalytic reaction. The most commonly used catalyst supports include metal-organic frameworks (MOFs), carbon, alumina, silica, and zeolites [58–60]. Catalytic substances are usually applied to porous structures through methods such as ion exchange, impregnation, or co-precipitation [61]. The process of exchanging metal ions is typically used to modify the acidity and/or pore size of zeolites.

Zeolite is a popular and valuable catalyst support material due to its highly organized micropore structure, high thermal stability, adsorption, and ion exchange characteristics [32]. The open-porous nature of Zeolites allows them to hold a wide range of exchangeable cations. If the size of the pores of Zeolites is similar to the molecules undergoing the reaction, it makes them ideal catalysts. They can be used as "in situ" oxidation catalysts and selective adsorbents [33]. Zeolites are unique materials known for their ability to selectively adsorb molecules based on size, owing to their advantageous porous structure. Different zeolite frameworks have varying pore sizes, allowing some to preferentially accommodate larger molecules while others are designed for smaller ones.

The Faujasite (FAU) structure is one of the most frequently employed in catalytic oxidation [34]. Faujasite Y zeolites have been employed in a variety of chemical and catalytic applications, including adsorption, separation, petroleum refining, aromatic alkylation, petrochemical, environmental protection, and natural gas dehydration [35]. This is due to their superior characteristics, which include a huge surface area (over 900 m^2 g^{-1}) [36], large adsorption capacity [37], large pore volume (up to 0.5 cm^3 g^{-1}) [36], high porosity, great thermal stability (up to 800 °C) [36], 3D channel structure and a substantial ion exchange capacity [38]. For this study, Zeolite Y was selected not only for its notable characteristics but also due to the availability of an efficient synthesis method under laboratory conditions. Moreover, its pore size is sufficient to accommodate a phenol molecule once adsorption occurs.

Previous studies have proven that Zeolites with transition metal ions are effective catalysts for the Fenton-like reaction, which oxidizes various organic contaminants [39–44]. The Fenton reaction is an advanced oxidation process that involves hydroxyl radicals. However, it's important to note that low-valence transition metal ions like Fe^{2+}, Cu^{2+}, and Co^{2+} are well-known oxidative Fenton's reagents that use hydrogen peroxide as an oxidant [31]. These cations are firmly bonded to exchange sites within the pore structure and are unlikely to leach out or precipitate during the process. If the size of the zeolite's pores is large enough to allow the reaction to proceed inside them, it's reasonable to assume that the transition metal ions transferred into the cages and/or channels of the zeolite could serve as the oxidant for phenol degradation [31]. Therefore, FAU Zeolites containing transition metal ions have been shown to be efficient catalysts in the oxidation of a range of organic pollutants through the Fenton-like reaction.

In research on the degradation of phenols, Fe^{2+} has been the most commonly used cation [24,40]. However, in this work, we focus on Cu^{2+} because it is more stable than Fe^{2+}, less toxic, and not easily converted into a hydroxide. It is also an excellent alternative to Fenton-like reactions because it can exhibit Fenton-like oxidation activity even at neutral and nearly neutral conditions [33]. Further, compared to iron, copper is a more effective catalytic material due to its unique properties. It can quickly interconvert Cu^{+} into Cu^{2+} and vice versa, and also form transient complexes with oxidation products. As oxidation products and copper do not permanently combine, the active sites remain available for the ongoing catalytic cycle. Consequently, copper is involved in the mineralization of organic materials and provides a superior redox cycle [45]. Copper has been reported as one of the most active species among various non-noble metals [46]. The ion exchange method is frequently used to synthesize the cation catalyst, which in turn alters the zeolite pore size and its acidity. While copper is exchanging with zeolite, a relationship with the zeolite acid strength can be observed. Literature suggested that cage-type zeolites, such as faujasite zeolites with strong acidity, can provide stability to copper ions [47]. The incorporation of copper into Zeolite-Y not only enhances redox activity but also introduces Lewis acid sites that can facilitate VOC activation.

The efficiency of phenol degradation using zeolite catalysts can be impacted by various environmental factors, such as moisture, temperature, and the presence of other gases. These atmospheric conditions can alter the catalytic behavior of zeolites, either by enhancing or inhibiting the adsorption and subsequent degradation of phenols. Despite the growing body of research on phenol degradation, the specific impact of altered atmospheric conditions on the performance of zeolite catalysts remains underexplored. However, only a few studies have delved into the effects of changing atmospheric conditions on catalysts during the degradation process [7,10,11,48,49]. But in all these studies, they have not validated their results by comparing them with those under an inert environment. It is also important to study phenol degradation under inert conditions to make comparisons. Also, there appears to be a shortage of research on the degradation of phenol vapor or in the gas phase in comparison to that of phenols in water, and the mechanisms involved in vapor phase degradation are not well-defined [15,20,21,46,50–54]. The challenges, such as controlling concentrations, analyzing, and monitoring results in gas-phase reaction analysis, may be the cause of this shortage of research. Although there are some studies with gaseous vapors, those have been conducted with expensive and complex experimental setups.

This study aims to address the above-mentioned research gaps by systematically investigating the effect of different atmospheric environments on the degradation behavior of phenol vapor via copper-modified Zeolite Y catalyst using a convenient but accurate experimental setup. This study hypothesizes that atmospheric conditions critically influence phenol degradation efficiency over zeolite catalysts. Increased moisture is expected to suppress degradation due to competitive adsorption of water molecules on active sites, whereas the introduction of oxidizing agents such as oxygen or hydrogen peroxide is predicted to enhance degradation by supplying additional oxidative pathways. Thus, the main objective of this study is to identify the suitable reaction conditions for the degradation of phenol vapor via zeolite catalysts in environmental applications. Moreover, this article provides a comprehensive understanding of the mechanism of the derivation and conversion of phenol vapor into degradation products.

2. Materials and methodology

2.1. Materials

NaOH (Pellet, Sigma Aldrich, ACS reagent, > 98 %), $NaAlO_2$ (Sigma Aldrich, reagent grade), LUDOX® AS-40 colloidal Silica (40 wt. % suspension in H_2O; Sigma Aldrich), NH_4NO_3 (Duchefa Biochemie, >97.5 %), $Cu(NO_3)_2.2{\cdot}5H_2O$ (Sigma Aldrich, ACS reagent), Phenol (VMR Chemicals, ACS), Methanol (Sigma-Aldrich, ACS reagent, > 99.8 %, GC)

2.2. Preparation of Zeolite CuY catalyst

Zeolite Y was synthesized via a hydrothermal (HT) seed-assisted method. First, the seed gel of Zeolite Y was prepared using 3.1606 g of $NaAlO_2$ dissolved in 11.2566 g of deionized water ($d = 1$ g cm^{-3}). Then 22.9821 g of 40 % (w/w) colloidal silica was added and stirred at room temperature for one day at 350 rpm. Next to prepare feed gel, 2.8212 g of NaOH and 4.0653 g $NaAlO_2$ were mixed in 48.6800 g deionized water ($d = 1$ g cm^{-3}) with magnetic stirring at 250 rpm. After the clear solution was obtained, 31.2375 g of 40 % (w/w) colloidal silica and 3.0589 g of seed gel were added and stirred [55,56]. After that, it was kept for 24 h to age. Next, the hydrothermal synthesis was carried out in this solution at 100 °C for 24 h in a Teflon container of the hydrothermal reactor. The resultant product (HT-Zeolite NaY) was washed using deionized water until the solution pH became neutral (pH around 7–8). Hydrogen Zeolite (HT-Zeolite HY) was synthesized according to the method given in [56,57] with slight modifications. For that, 1 g of HT-Zeolite NaY was stirred in 100 mL of 1 M NH_4NO_3 for two hours at 80 °C. Then it was dried at 120 °C for 4 h. Thereafter, the material was calcinated at 550 °C for 5 h. Calcinated Zeolite HY was subjected to three sequential cation modification processes with a 3:1 mass ratio of Zeolite HY to metal salts ($Cu(NO_3)_2.2{\cdot}5H_2O$. The mixture was stirred at 380 rpm in 60 mL DI water at 65 °C for a day. The material was filtered, and it was vacuum dried at 70 °C for 24 h. Thereafter, copper-modified Zeolite Y (HT-Zeolite CuY) was washed to remove excess metal salts and dried at 100 °C. Finally, the pure catalyst was obtained after calcination at 500 °C for one hour.

2.3. Characterization of the catalyst

HT-Zeolite CuY was characterized using Fourier Transform Infrared Spectroscopy (FTIR); Thermo Scientific NICOLET iS50 FT-IR, USA, Raman Spectroscopy; Renishaw inVia Raman Microscope, UK, Powder X-ray Diffraction (PXRD); Rigaku Ultima IV X-ray diffractometer, USA, Particle size analysis; HORIBA scientific nano particle NANO PARTICLE ANALYZER SZ-100, Japan, BET surface analysis; BELSORP MINI X, Microtrac BEL Corp, Japan, X-ray photoelectron spectroscopy (XPS); ESCALAB 250Xi, USA, Inductive Coupled Plasma/ Optical Emission Spectrometry (ICP/OES); Thermo Scientific iCAP 7000 series, USA, Scanning Electron Microscopic analysis (SEM); ZEISS EVO LS15, Germany and ZEISS EVO 18 and Bruker Quantax EDS, USA, and Energy Disperse X-ray spectrometry (EDS); ZEISS EVO 18 and Bruker Quantax EDS, USA.

2.4. Optimizing conditions and parameters of the phenol degradation

To optimize catalytic reaction conditions, such as time, temperature, etc., and degradation products analysis was done using the Shimadzu GC/MS-QP2010 ultra series model with a capillary column (Rtx®−624, 30 m, 0.25 mm ID, 1.4 μm df). The 1 μL injection volume in the split mode and the column oven temperature rise from 35 to 210 °C within 19.58 min. He (4.6 grade) was used as the carrier gas, and the flow rate was 24.8 mL/min. The Headspace (HS) analysis was performed using a Shimadzu HS-20 headspace sampler.

A phenol solution was prepared in GC-grade methanol with a 4 mM concentration. Therefore, the chromatogram was collected with a 2.5 min solvent cut. Then, 200 μL of phenol solution and 8 mg of HT-Zeolite CuY catalyst were placed in HS vials of the GC/MS-QP2010 series under a nitrogen gas environment. Then these vials were sealed and were heated up to 50, 75, 100, 125, and 150 °C. The GC/MS results were taken from each vial after one hour of heating. With those results, the optimum temperature of 100 °C was obtained. Under this optimum temperature, the phenol solution volume was optimized, considering 25, 50, 100, 200, and 400 μL volumes into separate HS vials and repeating the next steps above.

The catalyst dosage was optimized by taking 2, 4, 6, 8, and 10 mg of HT-Zeolite CuY. To optimize reaction time, samples were heated for 30, 60, 90, 120, and 150 min. Finally, the concentration of phenol solution was optimized under 100 °C for one hour by taking into account 1.0, 2.0, 3.0, 4.0, and 5.0 mM concentrations.

The percentage removal of phenol was calculated according to the equation given below; Here C_0 and C_f are the initial and final vapor phase concentrations of phenol, which were quantified after performing phenol standard sample calibration.

$$Percentage\ Removal\ of\ Phenol = \frac{(C_0 - C_f)}{C_0} \times\ 100\% \quad (1)$$

2.5. Degradation product analysis under various reaction environments

Under the aforementioned optimal conditions, GC/MS degradation products analysis was performed. Then, the reaction environment was altered to incorporate inert gas, moisture, and oxygen. Additionally, analysis of the degradation products was done when 3 % H_2O_2 was available in the reaction medium. The resulting chromatograms were subjected to post-run by SCAN acquisition mode (TIC scan range =

35–260 m/z) for qualitative analysis, and library data (NIST 115) was used as a library to compare individual compounds with standard chromatograms for degradation products identification. Comparing retention times (t_R) with those of authentic products facilitated the identification of intermediates during the phenol oxidation by the CuY catalyst. Fig. 1 shows the diagram of GC/MS analysis done with HS vials.

3. Results and discussion

3.1. Characterization of synthesized HT-Zeolite CuY

3.1.1. FTIR spectroscopy

FTIR data were collected from Nicolet IS50 FTIR spectrometer by the standard KBr pellet method, scanning from 400 to 4000 cm^{-1}. The instrument resolution is 4 cm^{-1} and spectra were designed and analyzed using Origin 2019 software. Fig. 2(a) represents the FTIR spectra of Zeolite CuY synthesized from hydrothermal (HT).

In the spectra, bands around 460, 820, 1050, 1100, 1650, and 3500 cm^{-1} correspond to the Zeolite Y structure commonly found in many publications [37,58–62]. The bands at 820 and 460 cm^{-1} are characteristic of the Si-O symmetrical stretching and bending vibration. The bands about 1100 and 1050 cm^{-1} belong to the external and internal T-O (T = Si, Al) asymmetrical stretching vibration, respectively [63,64]. Also, a small band appears around 600 cm^{-1} in the Zeolite CuY spectrum, and this band represents the loading of cation, and it may be due to the internal deformation vibration modes of T-O-T bridging bonds [65]. This indicates that copper cations have been incorporated into hydrothermally synthesized Zeolites (HT-Zeolite CuY). The presence of broadband around 2980–3700 cm^{-1} could be assigned to the O—H stretching mode either from H_2O or (Si-OH). The spectrum of HT-Zeolite CuY shows peaks at high frequencies around 3425 cm^{-1} and 3519 cm^{-1}, which could be seen due to Cu-OH vibrations and acidic hydroxyl groups [66,67].

3.1.2. Raman spectroscopy

The Renishaw inVia Raman Microscope was used to collect Raman data. Fig. 2(b) shows the Raman Spectra of HT-Zeolite CuY; the spectral region 100–2000 cm^{-1} is selected for the analysis. The predominant peak appeared in the range of 1200–1400 cm^{-1}. These bands are generally ascribed to the asymmetric stretching vibration of the Si-O bond [68]. This highest intensity peak is broader than the other peaks. Broadening is attributed to the disorder in the Al distribution [69]. So, from this observation, it can be suggested that copper cations may be incorporated into the Al sites. Further in the Zeolite CuY spectra, some bands below 120 cm^{-1} could be seen, and peaks at 110 cm^{-1} in HT-Zeolite CuY. These occur due to translational motions of intra-zeolite charge--balancing extra-framework cations. The broadening of these bands corresponds to the translational motion of the extra-framework cation [69]. However, the appearance of these bands is smaller than that of bands around 1200–1300 cm^{-1}; so that when copper is modified with Zeolites, the Al incorporation mechanism predominates would be suggested.

3.1.3. SEM and EDS analysis

Scanning Electron Microscopy images were obtained from ZEISS EVO LS15, Germany, to analyze the surface morphology of the synthesized microstructure of the samples. The samples were attached to conductive carbon scotch tape and covered with a 20 nm-thick gold layer. SEM images were taken using secondary electron mode at 20 keV. Fig. 2(c) shows the SEM images with the characteristic morphology of HT-Zeolite after copper modification. The regular octahedral shape of Faujasite Zeolite Y can be observed in HT-Zeolite CuY [37]. The reason for the defects may be the high-temperature calcination during cation incorporation. However, a highly crystalline morphology was observed in the SEM image of HT-Zeolite CuY, and its crystals are clearly visible.

The elemental chemical analyses are performed by using Bruker Quantax EDS, Energy Dispersive X-ray Spectrometry at a constant voltage of 20 keV with 20 k X magnification under a 1 mm area (Figure S1 and Figure S2). The samples are deposited on a stainless-steel holder and sputtered with gold.

The results of the elemental analyses given in Table 1 show the Si/Al ratio of 1.99, which corresponds to a unit cell formula of $(H_2O)_x[(AlO_2)_{64}(SiO_2)_{128}]$ for parent Zeolite HY [70]. The Si/Al ratio increases when the cation is incorporated, indicating mild dealumination during the exchange process [47]. According to the author H. Wang et al [47], during this process, aluminum may separate with copper incorporation and enter the solution as $Al(OH)_3$, then reattach to the zeolite's exterior during the drying process. This results in different Si/Al ratios, indicating the type of dealumination that occurs during Cu exchange.

3.1.4. PXRD analysis

Powder X-ray diffraction (PXRD) patterns of the samples were obtained with λ=1.54 Å Cu/Kα radiation and within the range 5 - 80° using a Rigaku Ultima IV X-ray diffractometer with CuK_α radiation (50 kV, 40 mA) at a scanning speed of 2 °/min. The crystallinity and purity of the synthesized zeolite phases were evaluated from these data. Fig. 3 shows PXRD patterns of (a) HT-Zeolite HY and (b) HT-Zeolite CuY. The peak pattern of as-synthesized HT-Zeolite shows similar patterns obtained

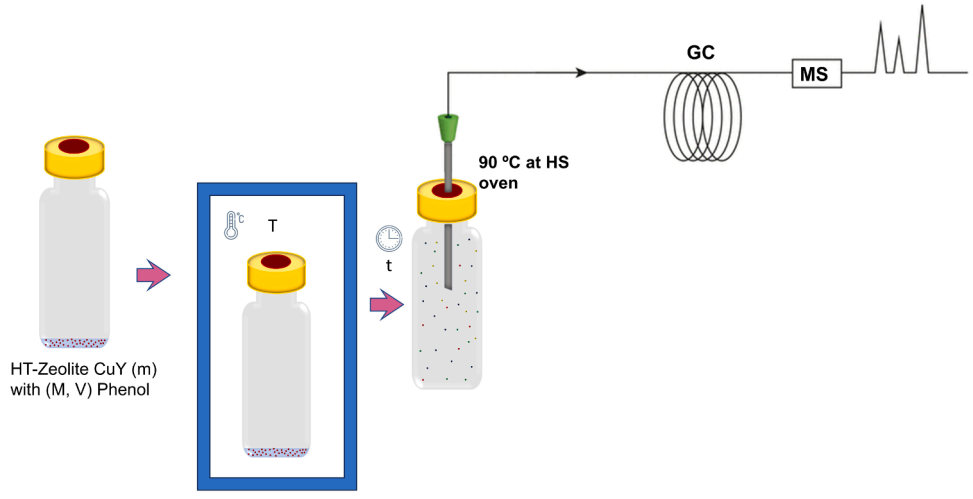

Fig. 1. Diagram of GC/MS analysis done with HS vials under reaction conditions of: V volume of M molar phenol solution, adding m dosage of HT-Zeolite CuY and oven heating at T temperature for t time.

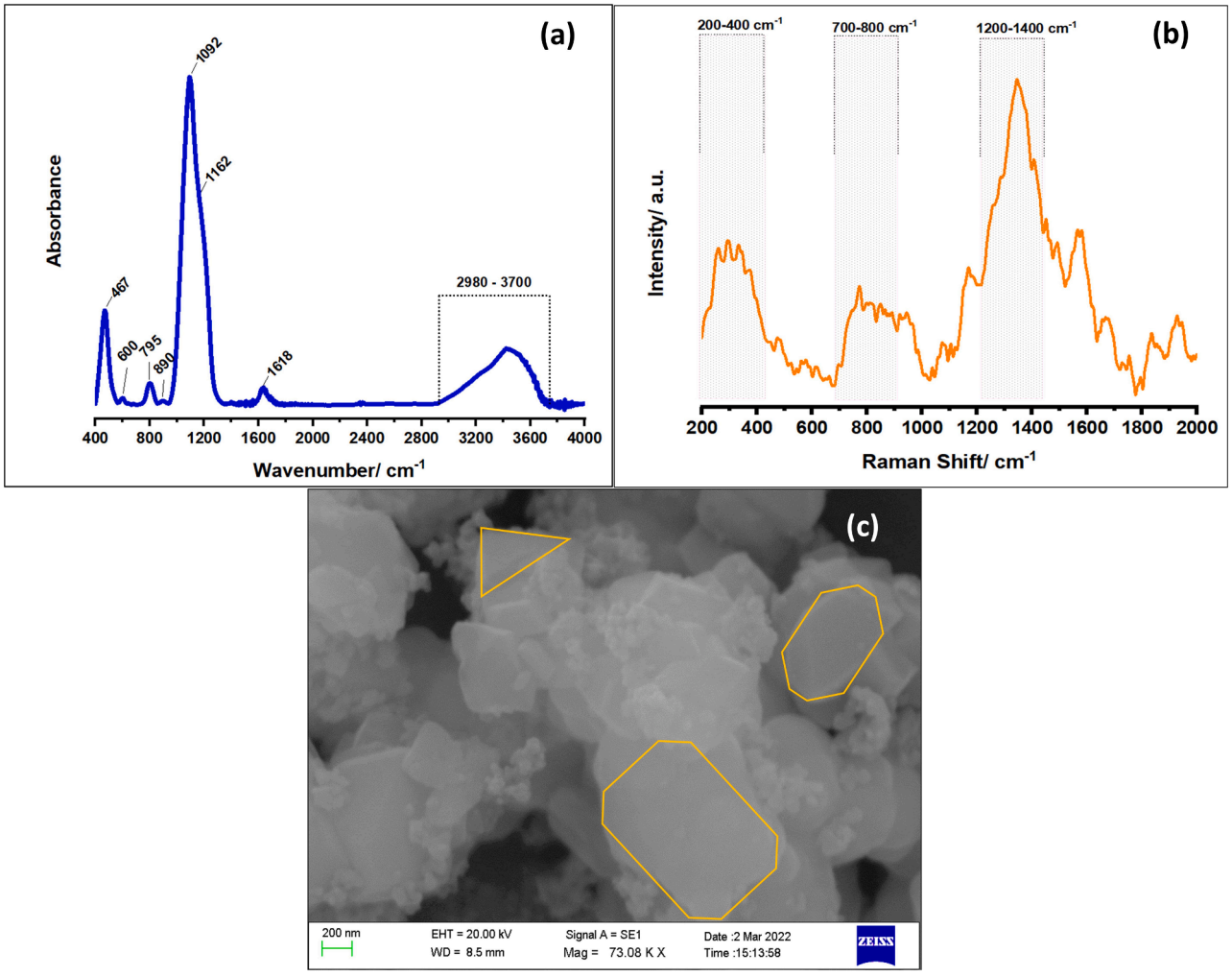

Fig. 2. Characterization data of HT-Zeolite CuY; (a) FTIR spectra range from 400–4000 cm^{-1}, (b) Raman spectra range from 100–2000 cm^{-1}; the inset is Raman shift range from 100–120 cm^{-1}, (c) SEM image at 20 keV with 73 K X Magnification.

Table 1
Elemental analysis by EDS and calculated Si/Al ratios of synthesized Zeolites.

Sample	Percentage of Elements				Si/Al
	Si	Al	O	Cu	
HT-Zeolite HY	25.73	12.94	61.33	NA	1.99
HT-Zeolite CuY	24.70	9.81	60.10	5.39	2.52

NA- not applicable.

from the Collection of Simulated XRD Powder Patterns for Zeolites database [71].

HT-Zeolite HY (before copper modified) spectrum reveals sharp peaks at 6.22, 10.16, 11.92, 15.68, 18.72, 20.42, 23.76, 27.14, 31.52, 34.18° corresponding to (111), (220), (311), (331), (511), (440), (533), (642), (555) and (840). HT-Zeolite CuY presents d values in 6.32, 10.28, 12.04, 15.82, 18.88, 20.56, 23.90, 27.28, 29.9, 31.02, 31.66, and 34.38° These peak values have shifted to a relatively higher angle than peaks in the PXRD pattern of Zeolite HY. For this phenomenon, an explanation has been provided in [63] with the aid of Bragg's equation. Peaks shift to a higher angle, suggesting a shrinkage of the unit cell parameter as θ is inversely proportional to the d value, which is directly proportional to a_0 (calculations are available in SI). Hence, upon copper modification, copper cations may be incorporated into the Al sites. Then, the changes that occur in the framework caused by the presence of these additional cations impact the overall structure of the Zeolite crystal and tend to shrink the structure. This result has been proven based on the Raman spectra in this study. As part of the HT-Zeolite HY matrix, copper cations are incorporated into the Al site by distorting octahedrally coordinated aluminum at Lewis acid sites [72,73].

The FAU Structure showing cation sites is in Fig. 4. Copper ions prefer to locate at Site $S_I/S_{I'}$ (SOD cage) and Site II on the surface or matrix of 12MR (FAU super cage) rather than highly coordinated Site III. Site preferences are $S_I > S_{II} > S_{I'}$ for monovalent $S_I > S_{I'} > S_{II}$ for divalent cations. However, Cu^+ can locate and stabilize in 6MR at D6R of the FAU framework, as it is difficult to reduce when it is in D6R [47]. Peak intensities of 220 and 311 reflections appear at 2θ=10 and 12°, respectively. In the PXRD pattern of HT-Zeolite HY $I_{220}<I_{311}$, while in the HT-Zeolite CuY pattern, $I_{220}>I_{311}$. This reveals the presence of the cation within the Zeolite Y super cage [64,74]. This observation is evidence for the exchange of Cu atoms in the super cage of Zeolite Y.

According to the PXRD patterns of Zeolite HY and Zeolite CuY, it can be seen that they are not very identical, so while copper ion incorporates with the Zeolite HY structure, structural modification occurs upon cation incorporation. The structural composition of zeolites is collectively modified by subsequent processes upon their incorporation of copper cations, thereby influencing their chemical and physical characteristics. During ion exchange processes, copper cations replace existing cations in the zeolite structure, introducing Cu species into the framework [75]. As a result of being confined within the zeolite pores, copper interacts with the zeolite structure to create a distinct

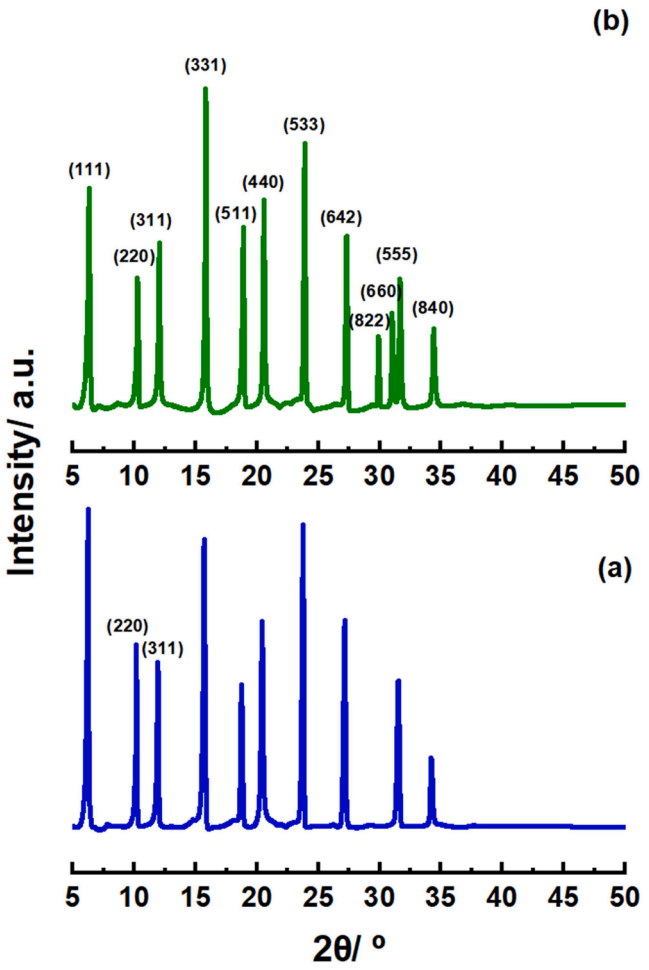

Fig. 3. PXRD patterns of (a) HT-Zeolite HY and (b) HT-Zeolite CuY range from 5–50°.

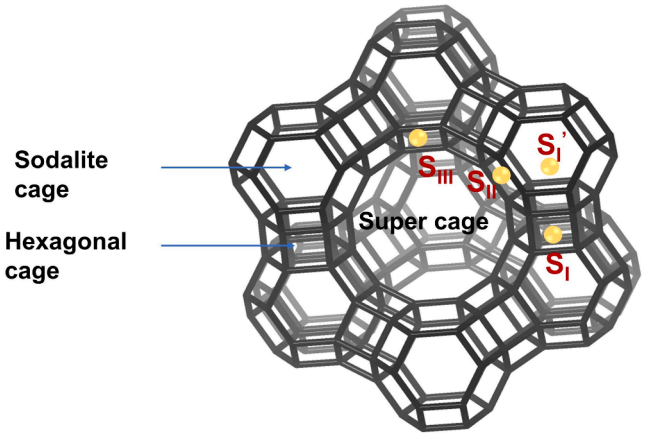

Fig. 4. FAU Structure showing cation sites [34].

coordination chemistry [76]. The preferences of copper cations for specific sites within the zeolite framework led to cation ordering effects, such as their affinity for 6-membered ring sites over 8-membered ring windows [77]. The incorporation of copper may also cause dealumination or changes in surface properties, impacting the structure and stability of the zeolite [78]. By generating active sites and interacting with reactants, copper can enhance the reactivity of zeolites, thereby influencing their catalytic properties [76].

Further, PXRD patterns after the cation modification (especially in HT-Zeolites) show a lowering in the peak intensities, and this could be caused by structural deformation occurring during Cu^{2+} exchange into Zeolite HY or the interaction of this cation with the framework oxygen of zeolite. The region of 2θ values at 10 and 20 has been considered to be correlated with the locations of cations in the Zeolite framework. Reduction of the characteristic peak indicates a redistribution of the intra-zeolite charge-balancing cation. Therefore, as observed in Raman data, some copper ions have been incorporated into extra-framework cation sites [79].

Then, according to the above observed PXRD patterns, it can be concluded that the copper cation has successfully incorporated into some Al sites and extra framework cation sites in the super cage of Zeolites, which are synthesized using the hydrothermal method.

3.1.5. XPS analysis

XPS was performed to analyze the chemical composition of the catalyst surface and to study the nature of the copper cation. So, the XPS measurements were carried out by an XPS (ESCALAB 250Xi), Thermo Fisher, USA system equipped with a scanning microprobe X-ray source (Monochromatic Al Kα 1486.7 eV X-rays), an electron flood gun, and a floating ion gun generating low-energy electrons (1:1 technique), respectively. The Origin software was used to perform Gaussian function deconvolution of the spectra. All relevant peaks for elements in zeolite, such as O 1 s, Si 2p and Al 2p, were fitted, and $2p_{1/2}$ and $2p_{3/2}$ peaks of Cu^{2+} and Cu^{+} were fitted as in Fig. 5.

Characteristic deconvoluted peaks with binding energy 529.4–530.8 eV can be attributed to lattice oxygen, while peaks at 531.7–532.2 eV are associated with surface oxygen or can be adsorbed oxygen or oxygen ions with low coordination state or oxygen atoms in hydroxyl groups [80]. Therefore, for O 1 s observed peaks at 531.93, 532.03, and 530.58 eV can be assigned to the oxygen atom from Si-O-Al linkage, Si-O-Si linkages, and O—Cu^{+} bond, respectively [74]. In the Si 2p core level, a major fitted peak at 102.82 eV has been assigned to SiO_2, and another peak at 102.48 eV can be assigned to Si_2O_3. The presence of Al_2O_3 is confirmed by the peak appearing at 74.84 eV, which is attributed to Al 2p [74].

At the Cu 2p core level, the binding energies for Cu $2p_{3/2}$ and Cu $2p_{1/2}$ of cuprous ions were found at 933.14 eV and 952.93 eV, respectively. Because Cu^{+} is sensitive to O_2, it is not surprising to find weak signals for cupric ions (Cu $2p_{3/2}$ and Cu $2p_{1/2}$) at 936.18 eV and 955.32 eV and as well as a satellite peak at 944.08 eV that represents the key properties of Cu^{2+} [47]. The presence of Cu(II) species, which characterise the d^9 configuration in the ground state, is indicative of the presence of this shake-up satellite peak [42,81]. These findings indicate that most of the copper in the catalyst exists in the (+1) oxidation state [74]. Upon heating, Cu^{2+} is converted to Cu^{+}, resulting in the formation of Cu^{+} species [42]. The observed energy difference of 19.79 eV between the two peaks agrees well with the 19.8 eV reported previously [42]. Based on the HT-Zeolite CuY XPS spectra, it is apparent that there are different oxidation states of copper on the support surface. This suggests that the HT-Zeolite CuY catalyst contains both monovalent and divalent copper.

According to all characterization results, it has been confirmed that the desired zeolite framework has been obtained from Hydrothermally synthesized Zeolite CuY. Table 2 represents the other important physicochemical properties of HT-Zeolite CuY based on the characterization data obtained.

3.2. GC/MS results for phenol degradation

3.2.1. Phenol conversion under inert (Anaerobic) conditions

The reaction conditions for the degradation of phenol were systematically optimized by evaluating several parameters, including temperature, volume of the phenolic solution, catalyst dosage, concentration of the phenol solution, and duration of the reaction. The results of these optimizations are detailed in Table 3.

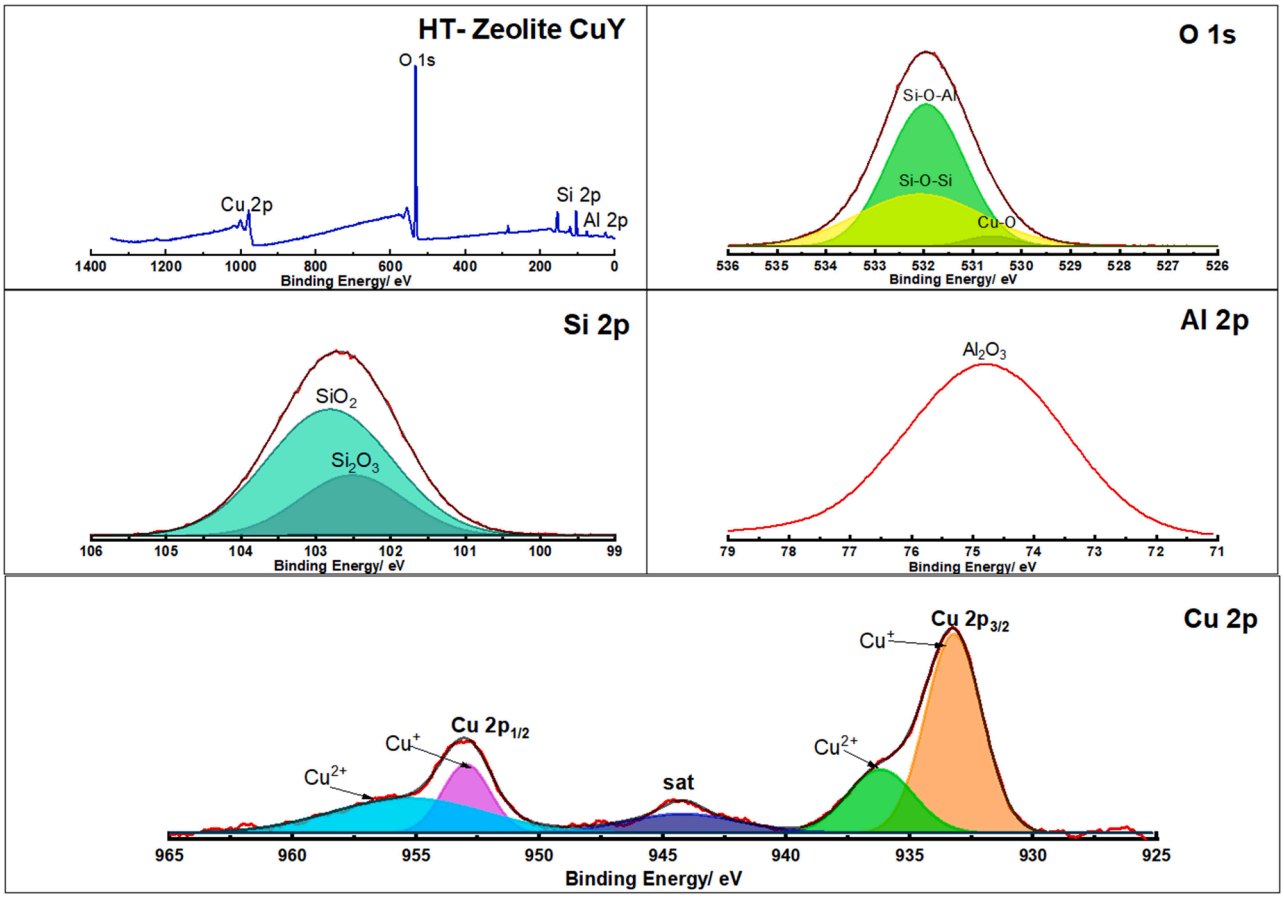

Fig. 5. XPS binding energy peaks for elements in HT-Zeolite CuY such that O 1 s, Si 2p, Al 2p and $2p_{1/2}$ and $2p_{3/2}$ peaks of Cu^{2+} and Cu^{+}.

Table 2
Physicochemical properties of synthesized HT-Zeolite CuY.

Average Particle Size (D_{50}) / μm	Crystal Size [a]/ nm	Crystallinity [a] /%	S_{BET}/ $m^2\ g^{-1}$	V_{micro}/ $cm^2\ g^{-1}$	SiO_2/ Al_2O_3 [a]
4.320	342.49	94.68	505	0.24	21.901

[a] Based on PXRD data. Calculations are available in the SI document.

Table 3
Optimized parameters for the phenol degradation via HT-Zeolite CuY under inert conditions.

Condition	Value
Temperature	100 °C
Phenol solution volume	100 μL
Catalyst dosage	8.000 mg
Phenol solution concentration	4 mM
Reaction time	60 min

Phenol degradation was evaluated using HT-Zeolite CuY under optimized anaerobic conditions, specifically within a nitrogen atmosphere. The results indicate a maximum phenol removal efficiency of 60.17 %.

3.2.2. Phenol conversion under moisture and oxygen/peroxide environment

This experiment examined the effects of phenol degradation in the presence of various atmospheric conditions, such as under oxygen (O_2), moisture, and hydrogen peroxide. It is found that the presence of moisture alone (Table 4, from the second row of the first column) leads to a lower percentage of phenol conversion/degradation than in the absence of any other stimulus (inert condition, Table 4, the first row of the first column). This is because water hinders phenol from degrading on many metal-based catalysts [80]. This could be due to the activity of the catalyst reducing or the competition between water and phenol for the active sites. Interestingly, the amount of phenol conversion significantly increased as the moisture content increased, but then decreased again when the moisture content continued to increase. Formation of H_2O^+ gas ions upon heating may tend to dissociate water molecules into ·OH at a moderate level of moisture [8] is one suggestion. Also, Cu^{2+} in HT-Zeolite CuY facilitates homolytic cleavage of water adsorbed near the site of the catalyst, forming surface-bound ·OH hydroxyl radicals or lattice oxygen species (Fig. 9). This may lead to an increase in the phenol conversion. This result could be further explained according to the density field maps study carried out by B. Ba Mohammed et al [82]. It appears that phenol molecules tend to be absorbed primarily in the center of broad intersections and larger channels like a super cage, while water molecules are equally spread within the small channels of Zeolite

Table 4
Phenol conversion with HT-Zeolite CuY under oxygen and/or moisture conditions.

Purge time of O_2 1.0 bar flow/min	0.0	1.0	2.0	3.0
Volume of H_2O/μL	Phenol Conversion/ %			
0.00	60.17	59.40	59.24	67.55
10.00	38.04	34.42	22.98	57.82
20.00	30.14	42.98	52.17	63.14
30.00	68.54	70.89	77.07	81.29
40.00	61.23	61.21	71.49	81.87
50.00	38.41	84.32	82.06	85.00

Y over the intersection. The energy values obtained from their research indicate that Zeolite Y has a stronger attraction for four phenol molecules compared to water, owing to its physical characteristics, such as its high hydrophobicity and the relatively lower polarity of phenol when compared to water [82]. However, high moisture levels again hinder the active sites of the catalyst.

In Table 4 (from the 2nd column of the first row), the percentage of conversion slightly decreased initially when oxygen was added in the absence of moisture, as compared to an inert state. However, with further purging of oxygen gas, the phenol conversion showed an increase. This is due to the oxidizing properties of oxygen, resulting in the production of more decomposition byproducts compared to an inert atmosphere. The presence of oxygen (O_2) can have an impact on oxidative degradation as it amplifies and overlaps with the reaction [40].

However, the addition of both oxygen and water to the reaction medium resulted in an increase in phenol conversion with increased moisture levels, but a decrease in conversion at low moisture levels. It can be suggested that when the presence of moisture and oxygen is at a moderate level, some hydroxy radicals may have been produced, which accelerates the phenol degradation. In this system, the presence of O_2, H_2O, and the zeolite catalyst enables surface contacts, hydrogen abstraction, and catalytic activity that collectively lead to radical production. Zeolite catalysts can assist in activating oxygen molecules. Reactive oxygen species (ROS) generated by the catalytic activation of O_2 can extract hydrogen atoms from water molecules, resulting in the formation of hydroxyl radicals (·OH). On the zeolite surface, water vapor (H_2O) and other molecules can competitively adsorb, causing localized concentration shifts and potentially promoting the production of radicals [83,84]. However, when increasing the moisture content, it may lead to a hindrance effect as discussed above.

The effect of phenol vapor degradation in the presence of H_2O_2 vapor has increased from 60 % to 94 % compared to inert conditions due to radical formation and auto-oxidation. Phenol conversion with the addition of peroxide and additional water vapor is given in Table 5. The percentage conversion has reached 94 % when moisture is absent, and as the above with oxygen, there's no decrease is observed with the addition of water. So, upon the addition of moisture, phenol has tended to fully convert to degradation products. It is obvious that the synthesis of ·OH radicals from peroxide brings the phenols to their degradation products. As reported data to completely oxidize 1 mol of phenol, 14 mol of hydrogen peroxide is required [85]. However, in the presence of a high amount of water vapor and peroxide vapor, the conversion has decreased from 99.9 % to 96.5 % and it may be due to the formation of hydroperoxyl radical (HO_2·), which has a little positive effect on the Fenton-like process [63] or hindrance effect from water vapor.

Fig. 6 displays a bar chart summarizing the average conversion of phenol under various reaction conditions. Even under inert conditions, phenol conversion/degradation occurs at an acceptable level. The addition of moisture, however, results in decreased conversion. On the other hand, introducing oxygen to the reaction vial leads to a slight increase in conversion. The increase becomes more significant with the addition of an oxygen and moisture mixture. As anticipated, the inclusion of peroxide results in increased phenol oxidation. Combining peroxide with moisture leads to nearly total phenol conversion.

Table 5
Phenol conversion with hydrogen peroxide and water via HT-Zeolite CuY.

30 % H_2O_2/ µL Additional Water/ µL	20.00 Phenol Conversion/ %	40.00	60.00	80.00	100.00
0.00	87.15	91.42	95.85	94.19	94.13
10.00	87.93	94.41	99.76	99.77	99.95
20.00	96.00	98.52	89.92	99.80	99.91
30.00	95.87	99.28	99.69	96.85	99.92
40.00	98.52	99.71	99.79	99.82	96.51

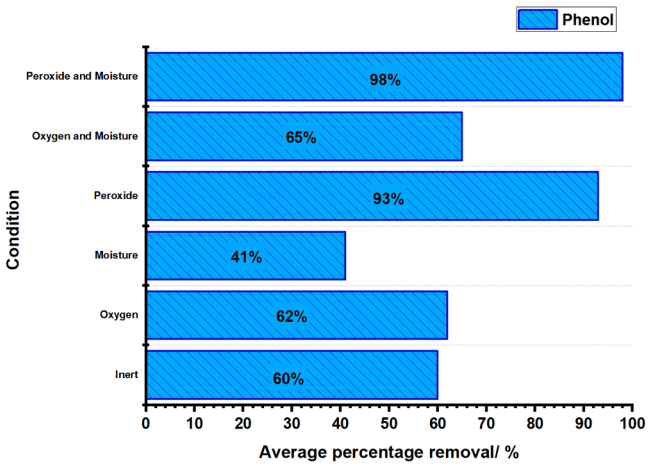

Fig. 6. Summary of the phenol conversion under different reaction conditions, such as inert, with oxygen, with moisture, with peroxide, with oxygen and moisture, and with peroxide and moisture.

3.2.3. *Degradation products analysis and mechanism study*

Ethanol, 2-butanol, 2-pentanone, and 3-pentanone are common degradation products obtained in inert, oxygen, and moisture environments. However, the formation of acetone can be seen in the moisture environment. Table 6 summarizes the products generated from the degradation of phenolic vapor under various modified conditions.

The phenol may be adsorbed in the pores of Zeolite Y through the hydroxyl group of phenol to the basic oxygen atoms of the terminal Si-OH in zeolite due to its acidity ($p^{Ka} = 9.89$) [82]. It is highly probable that, at high coverage, the Cu^+ ions will also interact with either the aromatic ring or the hydroxyl oxygen of phenol. Previous research has suggested that when the coverage is high, the interaction between the π-electrons of the aromatic molecule and the silanol terminal group, Si-OH may also be involved [82]. It is reasonable to assume that there are two different adsorption mechanisms through which phenol molecules can attach to the surface of zeolite. Phenol can adopt two orientations: one is vertical, where its hydroxyl group interacts solely with the surface, and the other is more parallel to the surface, where the aromatic ring interacts with the surface simultaneously [82]. In this study, we observed the formation of products like p-Benzoquinone within an inert atmosphere, suggesting that vertical interactions play a significant role in the phenol conversion mechanism with the HT-Zeolite CuY catalyst.

The copper ion is mostly located in the 3D channel (sodalite, main channel, and hexagonal prism) of the FAU structure (Fig. 4) [47]. Characterization results revealed that the exchange of Cu atoms could be within the super cage of Zeolite Y. The adsorbed phenol can diffuse into the crystal's interior, and could access the super cage (7.4 Å) due to its compatible size, with a kinetic diameter of 6.0 Å [86]. This 12-membered ring structure and its channels are spacious enough to allow all the products to diffuse out as well. But it is not possible to pass into the space inside the sodalite cage. The inter-crystalline Y zeolite pores contain both acidic protons and oxidative Cu^+/Cu^{2+} ions, which might be responsible for the high activity level observed in HT-Zeolite CuY [31]. The activity of acidic catalysts is controlled by Bronsted acidity, which causes hydrocarbons, in this case phenols, to adsorb on these sites and initiate the oxidation process [67]. Additionally, the catalytic activity of transition metal species is affected by the outer d-electron density [87]. The degradation reaction can occur within the inter-crystalline zeolite cages and channels situated in the super cage of the FAU structure. Then S_{II} can act as a potential active cation site, as this site is located at the six-membered ring, facing the super cage site in zeolite Y, as an exchangeable cation [31,73].

The catalyst has been treated with calcination before being used, which significantly improves its acidity and stability when exposed to

Table 6
Degradation products obtained from GC/MS after phenol vapor conversion with HT-Zeolite CuY at different reaction conditions, including inert, oxygen, moisture, and/or peroxide.

Inert air Condition	Oxygen Condition	Moisture Condition	Moisture and Oxygen Condition	H_2O_2 Condition	Moisture and H_2O_2 Condition
Ethanol	Ethanol	Ethanol	Ethanol	Ethanol	Ethanol
2-Butanone	2-Butanone	Acetone	3-Methyl Pentane	2-Propenal	Methylal
2-Propoxy Ethanol	2-Pentanone	2-Butanone	2-Butanone	Methylal	Acetone
2-Pentanone	3-Pentanone	2-Pentanone	2-Pentanone	Acetone	Acetic acid Methyl ester
3-Pentanone	Butanoic acid Methyl ester	3-Pentanone	3-Pentanone	Acetic acid Methyl ester	1,1-Dimethoxy Ethane
2-Methoxy Phenol	2-Ethyl-1-Hexanol	4-Methyl-1,3-dioxolane	2-Ethyl-1-Hexanol	1,1-Dimethoxy- Ethane	p-Dioxane-2,3-diol
p-Benzoquinone				Methyl vinyl ketone	2-Butanone
				p-Dioxane-2,3-diol	Formic acid
				2-Butanone	Acetic acid
				Formic acid	Methoxy acetic acid methyl ester
				Acetic acid	
				p-Benzoquinone	
				Methyl Propionate	

water. This treatment creates Lewis acidic sites within the zeolite pores by moving some of the lattice aluminium into a different position. It can be proposed that the unique lattice structure of the faujasite type indirectly promotes cooperation between Lewis and Brønsted acids, creating sodalite cages that effectively stabilize large cationic aggregates. When an activated intermediate interacts with the Lewis acidic sites, it promotes the ring-opening reaction, increasing the overall reaction rate [73].

In the inert environment, when phenol reaches the active site of the zeolite catalyst, as the copper cation draws electrons from oxygen on the zeolite, phenol O—H bond cleaving could be possible as H is attracted by the terminal oxygen of the Zeolite (Fig. 7). It will create a partial negative charge at the ortho and para positions of the benzene ring. Once the phenol is attracted to the copper cation site, the bond cleaving of the terminal Bronsted acid site can proceed to create radicals. Subsequently, the less hindered para position of phenol is attacked by OH radicals, and the benzoquinone intermediate is produced [45]. Fig. 7 and Fig. 8 schematically depict the potential pathway for phenol degradation. This suggestion was proposed because the reaction media does not contain any oxidizing agents, and therefore, the only oxygen that can be involved in the mechanism is terminal oxygen from the zeolite framework. In this context, it is possible for radicals to form from the zeolite framework. The success of phenol degradation depends on the oxidation state of metal ions in catalysts and the in-situ production of radicals such as ·OH, ·O, and/or $\cdot O_2$ [9]. Conversely, fewer intermediate products are seen in the inert environment.

Based on the Raman spectroscopic data and PXRD analysis, it was observed that some of the Al sites in the catalyst were disordered by Cu atoms. This substitution caused the development of surface oxygen defects, which led to an increase in the amount of oxygen adsorbed on the HT-Zeolite CuY catalyst. The presence of active surface oxygen defects may also lower the energy barrier required for the reaction to occur.

The hydroxyl radical (·OH) can remove hydrogen atoms from almost every C—H bond of organic complexes, as the O—H bond energy is higher than the majority of C—H bond energies, according to thermodynamics. At the aerobic condition, the first attack of ·OH generates

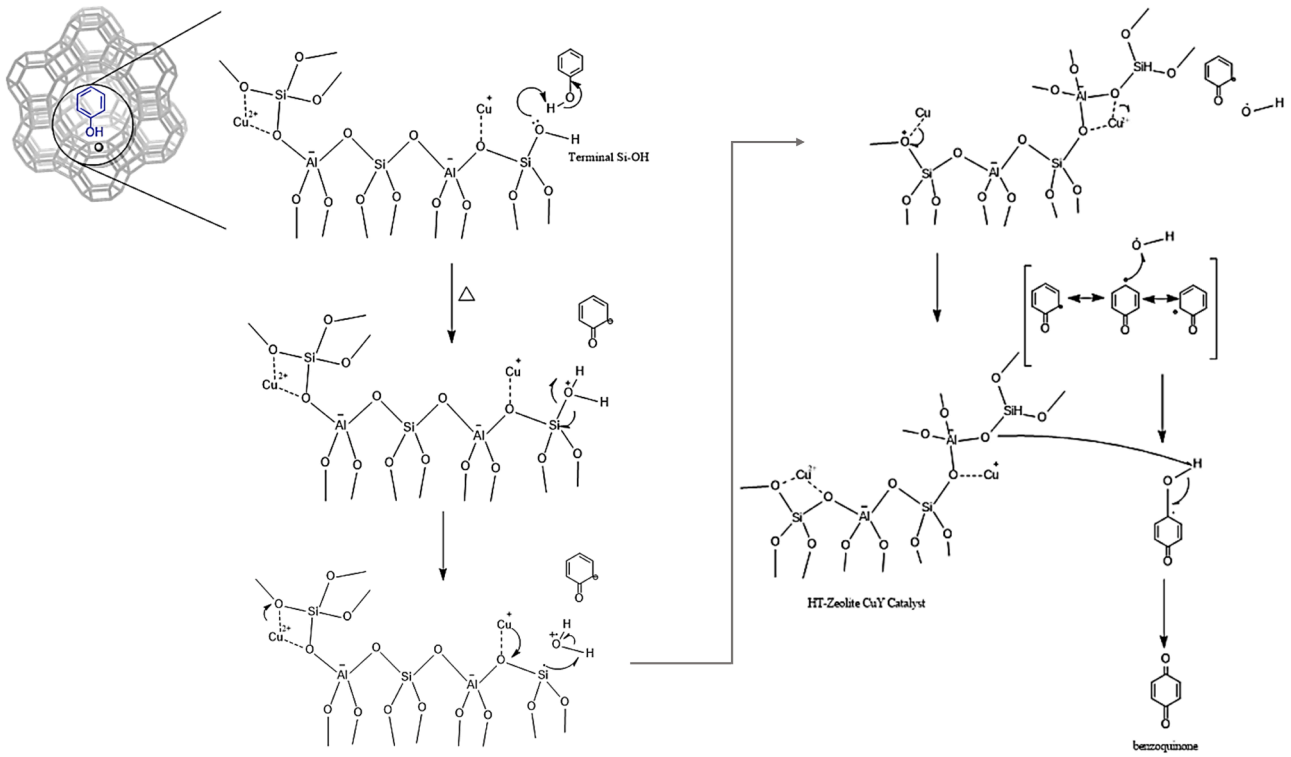

Fig. 7. Proposed mechanism for phenol degradation under the inert environment with HT-Zeolite CuY at the optimum reaction conditions; Temperature-100 °C, Phenol solution volume-100 μL, Catalyst dosage-8000 mg, Phenol solution concentration-4 mM, Reaction time-60 min.

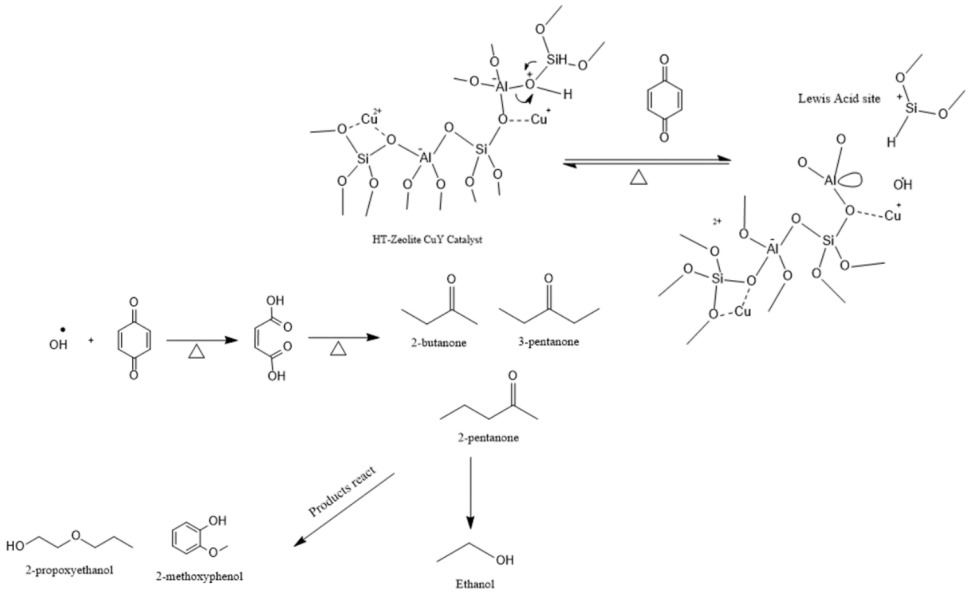

Fig. 8. Degraded product formation from phenolic vapor after catalytic degradation with HT-Zeolite CuY under inert conditions at the optimum reaction condition; Temperature-100 °C, Phenol solution volume 100 μL, Catalyst dosage-8.000 mg, Phenol solution concentration-4 mM, Reaction time-60 min.

carbon-centered radicals, which initiate a series of events resulting in the creation of organic peroxyl intermediates. To complete the process, molecular oxygen catches radicals with a carbon center or organic radical cations. Some C—C bonds break, causing degradative oxidation, resulting in oxidized compounds with fewer carbon atoms. Zeolite frameworks regulate the pH in the reaction medium, providing the conditions for the reaction to occur [40].

According to the discussion in Section 3.2.2, the mechanism of Phenol conversion when a moderate level of water presence is illustrated in Fig. 9.

Copper ions (Cu^{+}) can react with oxygen (O_2) in the presence of moisture to form a Cu-O-O radical. This radical can then react with phenol as shown in below reaction steps (2) to (7). Another pathway involves the reaction of Cu^{2+} with an intermediate that is produced after the phenol reacts with oxygen [88].

$$[Cu^{+}]\text{–Zeolite} + O_2 + H_2O \rightarrow [Cu^{2+}\text{–O–O}\cdot]\text{–Zeolite} + OH^{-} \quad (2)$$

$$C_6H_5\text{–OH} \rightarrow C_6H_5\text{–OH}\cdots[Cu^{2+}\text{–O–O}\cdot]\text{–Zeolite (OH)} \quad (3)$$

$$C_6H_5\text{–OH} + \text{Cu–O–O}\cdot \rightarrow C_6H_4(OH)(OOH)\text{–}Cu^{2+} \quad (4)$$

$$C_6H_4(OH)(OOH) \rightarrow \text{benzoquinone} \rightarrow \text{ring-opened dicarboxylic acids} \quad (5)$$

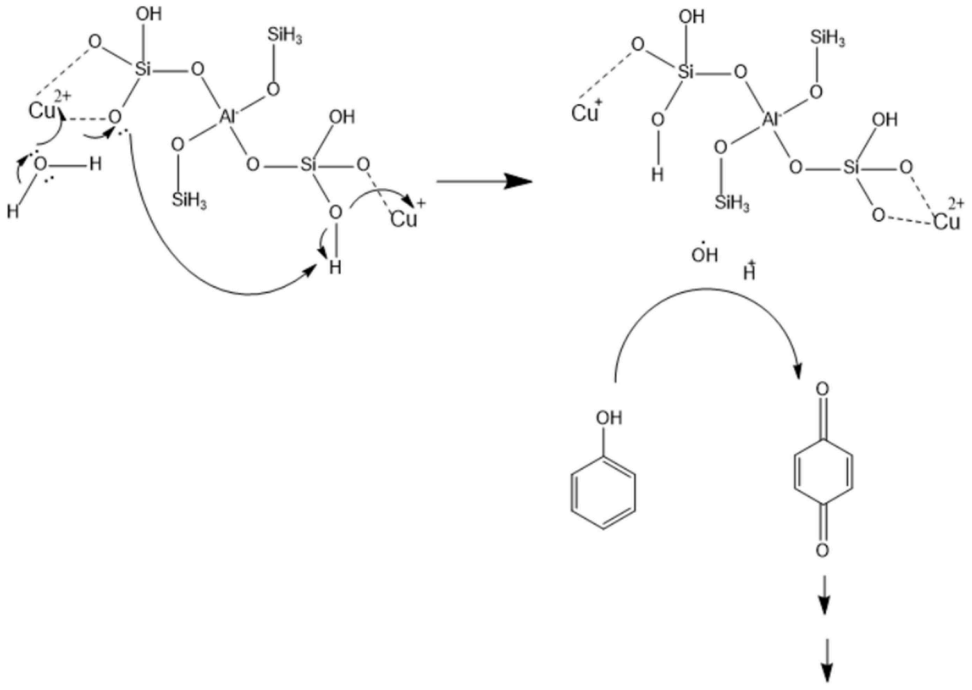

Fig. 9. Proposed mechanism of phenol degradation with HT-Zeolite CuY with the moisture under the optimum reaction condition; Temperature-100 °C, Phenol solution volume-100 μL, Catalyst dosage-8.000 mg, Phenol solution concentration-4 mM, Reaction time-60 min, H_2O. Reaction continuing is indicated with two short arrows, and product formation may be similar to Fig. 8.

$$Cu^{+} + O_2 \rightarrow Cu^{2+}\text{–}O_2^{-} \rightarrow Cu\text{–}O\text{–}O\cdot \quad (6)$$

$$Cu^{2+} + H_2O \rightarrow Cu^{+} + \cdot OH + H^{+} \quad (7)$$

The redox cycle between Cu^{+}/Cu^{2+} produces ·OH, which breaks down phenol through H_2O_2-mediated oxidation [54], and singlet oxygen ($^1O_2$) may be mainly produced through the surface oxygen defect path, and this involves phenol degradation [63]. The formation of specific oxidation products, such as hydroperoxides or oxygenated phenol derivatives such as benzoquinone, can indicate the presence of singlet oxygen ($^1O_2$) [89]. The molecular structure of phenol is related to its oxidative breakdown process. When a hydroxyl group replaces a hydrogen atom on the benzene ring, the electron cloud density becomes unevenly dispersed. Due to the larger electron cloud density during interactions with phenolic compounds, hydroxyl radicals initially attack the ortho or para position [54]. Then, the degradation of phenol in the presence of peroxide commences with the electrophilic addition of hydroxyl radicals to the aromatic ring, resulting in the development of polyhydroxylated benzene derivatives [54]. The process involves the conversion of phenol to hydroquinone and catechol, which then oxidize and give rise to o- and p-benzoquinone [24]. In the presence of a strong oxidant like peroxide in the media, hydroquinone is promptly oxidized to p-benzoquinone [24]. According to research findings, p-benzoquinone is an important intermediate product that forms during the degradation of phenol [20,63,85]. After the first reaction step, di-hydroxylated derivatives are oxidized to produce polyhydroxylated derivatives and/or quinones, which then undergo oxidative ring-opening reactions to yield carboxylic acids [24]. Higher amounts of formic acid and trace amounts of acetic acid are formed during the peroxide oxidation in this study, which agrees with the general mechanisms. However, Methylal is the major product among all these degradative by-products. The second major one is acetic acid methyl ester. Upon addition of more peroxide, p-benzoquinone peak intensity decreases, and methylal, acetic acid methyl ester, and formic acid peaks increase. This means ring opening and further oxidation happen upon the addition of more H_2O_2. The complete Fenton reaction produces CO_2 when single carbon atoms are formed. The possible reaction mechanism is illustrated in Fig. 10.

As a summary of this discussion, it can be suggested that when ion exchange occurs, the copper cation Cu+ is available at the active site of the catalyst's zeolite. Then it undergoes oxidation to Cu^{2+} by producing hydroxyl radicals from framework zeolite hydroxyls when it's subjected to heat. Then, a similar Fenton-type reaction happens partially for phenols even in inert air conditions. So, when phenol oxidizes, OH radicals reduce Cu^{2+} to $Cu^{+}$and the catalyst is regenerated. When oxygen is provided, the reaction is accelerated, and upon the addition of moisture, initial degradation increases, but further addition of water inhibits the oxidation of phenol. Then, it is obvious that the addition of H_2O_2 to phenol undergoes a full Fenton-like reaction at a high reaction rate. This implies phenol pollutants are decomposed in the external medium when the atmosphere is altered and within the zeolite framework under inert conditions.

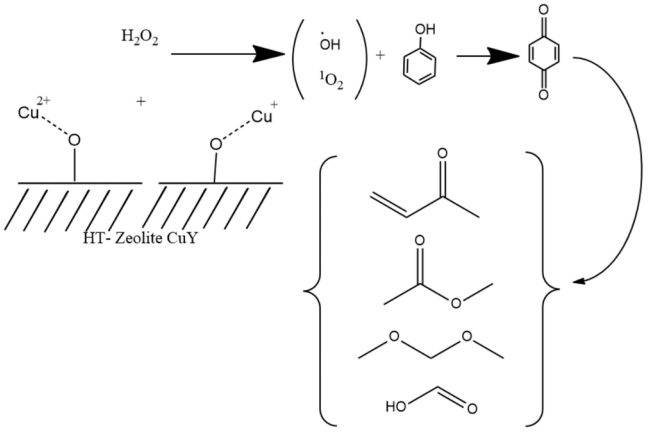

Fig. 10. Proposed mechanism of phenol degradation with HT-Zeolite CuY with the peroxide under the optimum reaction condition; Temperature-100 °C, Phenol solution volume-100 μL, Catalyst dosage-8.000 mg, Phenol solution concentration-4 mM, Reaction time-60 min, 3 % H_2O_2.

The mechanism described herein can be further verified through theoretical modelling in subsequent research on this topic. To minimize experimental variability, it is recommended that future studies be conducted in an inert glove box, to eliminate the influence of ambient VOCs. Additionally, other phenolic derivative degradation reactions and computational modelling are suggested to further elucidate the degradation mechanisms and validate the findings.

4. Conclusions

In this study, Faujasite zeolite was successfully synthesized via a seed gel-assisted hydrothermal method, and copper cations were effectively incorporated into the framework. The resulting HT-Zeolite CuY catalyst was applied for phenol vapor degradation under inert, humid, and aerobic conditions, as well as in the presence of H_2O_2. Unlike conventional flow systems, closed vials were employed, and volatile intermediates and by-products were analyzed using headspace gas chromatography.

Under inert gas conditions, the HT-Zeolite CuY catalyst achieved up to 60 % phenol conversion, with the acidic framework providing a favorable environment for degradation. Mechanistic insights derived from characterization and chromatographic data suggest that surface Si–OH groups play a key role in generating hydroxyl radicals, initiating a Fenton-type degradation pathway even under inert air. The introduction of oxygen further accelerated phenol conversion, while moderate moisture unexpectedly enhanced the initial degradation steps. The addition of H_2O_2 triggered a rapid and complete Fenton-like reaction, indicating that phenolic vapors can be degraded both within the zeolite framework and in the external reaction medium.

Overall, this work highlights the dual functionality of HT-Zeolite CuY as both an acidic and redox-active catalyst, demonstrating its potential for efficient phenolic vapor removal under a range of atmospheric conditions.

Funding

This research is funded by the National Institute of Fundamental Studies (NIFS), Kandy, Sri Lanka.

Consent for publication

All authors give their consent for publication.

CRediT authorship contribution statement

Lasanga Amarasena: Writing – original draft, Visualization, Validation, Methodology, Formal analysis, Data curation, Conceptualization. **Rohan Weerasooriya:** Writing – review & editing. **Athula Bandara:** Writing – review & editing, Supervision, Investigation, Data curation. **Xing Chen:** Data curation. **Lakmal Jayarathna:** Writing – review & editing, Validation, Supervision, Resources, Project administration, Investigation, Funding acquisition, Conceptualization.

Declaration of competing interest

The authors declare the following financial interests/personal relationships which may be considered as potential competing interests:

Lakmal Jayarathna reports financial support was provided by National Institute of Fundamental Studies. If there are other authors, they declare that they have no known competing financial interests or

personal relationships that could have appeared to influence the work reported in this paper.

Acknowledgement

This research is funded by the National Institute of Fundamental Studies, Kandy, Sri Lanka. Mr. Yohan Jayawardhana, a former research assistant at the National Institute of Fundamental Studies, provided the GC/MS instrument training and rubber septum for the HS vials. Author Lasanga Amarasena also acknowledges Ms. Anupama Amarasekara (former research assistant, NIFS) for assisting in GC/MS running. Furthermore, the authors acknowledge Hefei University of Technology, Hefei, China, for facilitating XPS analysis. The authors declare no competing interests or conflicts of financial interest.

Supplementary materials

Supplementary material associated with this article can be found, in the online version, at doi:10.1016/j.nexres.2025.101120.

Data availability

The authors declare that the data supporting the findings of this study are available within the paper and upon request.

References

[1] Y. Kharayat, V.K. Verma, B. Kumar, C.S. S, Phenol and Phenolic compound, CENTRAL POLLUTION CONTROL BOARD (Ministry of Environment, Forests & Climate Change), Delhi, 2016.
[2] M.A. Rubio, P. Bustamante, P.Y. Vásquez, Atmospheric phenolic derivatives AS tracers in an Urban area, J. Chil. Chem. Soc. 64 (2019) 4407–4411, https://doi.org/10.4067/S0717-97072019000204407.
[3] M. Li, X. Wang, C. Lu, R. Li, J. Zhang, S. Dong, L. Yang, L. Xue, J. Chen, W. Wang, Nitrated phenols and the phenolic precursors in the atmosphere in urban Jinan, China, Sci. Total Environ. 714 (2020) 136760, https://doi.org/10.1016/j.scitotenv.2020.136760.
[4] Atlanta, toxicological profile for Phenol. Atlanta (GA), agency Toxic Subst, Dis. Regist. (2008). https://www.ncbi.nlm.nih.gov/books/NBK599445/. accessed March 8, 2024.
[5] US enviromental protection agency, phenol hazard summary, phenol 1 (2000) 95–108.
[6] OSHA, permissible exposure limits – annotated tables, occup. Saf. Heal. Adm. (2017). https://www.osha.gov/annotated-pels/table-z-1 (accessed June 22, 2022).
[7] G. Moussavi, M. Mohseni, The treatment of waste air containing phenol vapors in biotrickling filter, Chemosphere 72 (2008) 1649–1654, https://doi.org/10.1016/j.chemosphere.2008.05.040.
[8] J.Z. Wahono, R.D. Yusharyahya, Harianingsih, N. Saksono, Phenol degradation by fenton reaction in air injection using plasma electrolysis method, IOP Conf. Ser. Mater. Sci. Eng. 980 (2020), https://doi.org/10.1088/1757-899X/980/1/012051.
[9] C. Lai, T. He, X. Li, F. Chen, L. Yue, Z. Hou, Catalytic wet air oxidation of phenols over porous plate Cu-based catalysts, Appl. Clay Sci. 181 (2019) 105253, https://doi.org/10.1016/j.clay.2019.105253.
[10] F. Arena, C. Italiano, A. Raneri, C. Saja, Mechanistic and kinetic insights into the wet air oxidation of phenol with oxygen (CWAO) by homogeneous and heterogeneous transition-metal catalysts, Appl. Catal. B Environ. 99 (2010) 321–328, https://doi.org/10.1016/j.apcatb.2010.06.039.
[11] C. Xu, L. Wang, Atmospheric oxidation mechanism of phenol initiated by OH radical, J. Phys. Chem. A 117 (2013) 2358–2364, https://doi.org/10.1021/jp308856b.
[12] M.K. Zamisa, T.W. Seadira, S.J. Baloyi, Transforming wastewater treatment: recent advancements in Catalytic Wet Air Oxidation with pillared clay catalysts for phenol remediation, Environ. Pollut. 361 (2024) 124842, https://doi.org/10.1016/j.envpol.2024.124842.
[13] R. Zhao, H. Wang, D. Zhao, R. Liu, S. Liu, J. Fu, Y. Zhang, H. Ding, Review on catalytic oxidation of VOCs at ambient temperature, Int. J. Mol. Sci. 23 (2022) 13739, https://doi.org/10.3390/ijms232213739.
[14] K. Akinlolu, B. Joshi, H. Raghav, P. Rawat, M. Kumar, B. Sarkar, S. Tripathi, Encaged Cu2+/Co2+ zeolite materials: efficient and reusable catalysts for oxidation of phenol, Curr. Res. Green Sustain. Chem. 5 (2022) 100310, https://doi.org/10.1016/j.crgsc.2022.100310.
[15] L.F. Liotta, M. Gruttadauria, G. Di Carlo, G. Perrini, V. Librando, Heterogeneous catalytic degradation of phenolic substrates: catalysts activity, J. Hazard. Mater. 162 (2009) 588–606, https://doi.org/10.1016/j.jhazmat.2008.05.115.
[16] N. Nunotani, A.R. Supandi, P.G. Choi, N. Imanaka, Catalytic liquid-phase oxidation of phenolic compounds using ceria-zirconia based catalysts, Front. Chem. 6 (2018) 1–6, https://doi.org/10.3389/fchem.2018.00553.
[17] Y. Liu, H. Lu, G. Wang, Preparation of CuO/HZSM-5 catalyst based on fly ash and its catalytic wet air oxidation of phenol, quinoline and indole, Mater. Res. Express 8 (2021), https://doi.org/10.1088/2053-1591/abd6a4.
[18] C.A. Pires, A.C.C. Dos Santos, E. Jordão, Oxidation of phenol in aqueous solution with copper oxide catalysts supported on γ-Al2O3, pillared clay and TiO2: comparison of the performance and costs associated with each catalyst, Brazilian J. Chem. Eng. 32 (2015) 837–848, https://doi.org/10.1590/0104-6632.20150324s00002232.
[19] C. Dai, A. Zhang, L. Luo, X. Zhang, M. Liu, J. Wang, X. Guo, C. Song, Hollow zeolite-encapsulated Fe-Cu bimetallic catalysts for phenol degradation, Catal. Today 297 (2017) 335–343, https://doi.org/10.1016/j.cattod.2017.02.001.
[20] I. Wysocka, E. Kowalska, K. Trzcinski, M. Łapinski, UV-vis-induced degradation of phenol over magnetic photocatalysts modified with Pt, Pd, Cu and Au nanoparticles, Nanomater. Artic. (2018), https://doi.org/10.3390/nano8010028.
[21] T. Setyaningtyas, K. Riyani, C. Firdharini, Photodegradation of phenol in batik wastewater with copper (II) oxide under visible light illumination, in: AIP Conf. Proc, AIP Publishing, 2020, https://doi.org/10.1063/5.0005354.
[22] L. Jay, E.E.M.N. Chirwa, Pathway analysis of phenol degradation by UV /TiO2 photocatalysis utilising the C-13 isotopic labelling technique Pathway analysis of phenol degradation by UV / TiO 2 photocatalysis utilising the C-13 isotopic labelling technique, (2018). https://doi.org/10.3303/CET1870031.
[23] L. Jay, E.E.M.N. Chirwa, Pathway analysis of phenol degradation by UV/TiO2 photocatalysis utilising the C-13 isotopic labelling technique, Chem. Eng. Trans. 70 (2018) 181–186, https://doi.org/10.3303/CET1870031.
[24] M. Pimentel, N. Oturan, M. Dezotti, M.A. Oturan, Phenol degradation by advanced electrochemical oxidation process electro-fenton using a carbon felt cathode, Appl. Catal. B Environ. 83 (2008) 140–149, https://doi.org/10.1016/j.apcatb.2008.02.011.
[25] NIEHS, Potential for Human exposure. Phenol Toxicol. Profile, National Institute of Environmental Health Science, 2006, pp. 149–172.
[26] R. Alnaizy, A. Akgerman, Advanced oxidation of phenolic compounds, Adv. Environ. Res. 4 (2000) 233–244, https://doi.org/10.1016/S1093-0191(00)00024-1.
[27] G. Liu, J. Ji, H. Huang, R. Xie, Q. Feng, Y. Shu, Y. Zhan, R. Fang, M. He, S. Liu, X. Ye, D.Y.C. Leung, UV/H2O2: an efficient aqueous advanced oxidation process for VOCs removal, Chem. Eng. J. 324 (2017) 44–50, https://doi.org/10.1016/j.cej.2017.04.105.
[28] P. Monneyron, S. Mathé, M.H. Manero, J.N. Foussard, Regenaration of high silica zeolites via advanced oxidation processes - A preliminary study about adsorbent reactivity toward ozone, Chem. Eng. Res. Des. 81 (2003) 1193–1198, https://doi.org/10.1205/026387603770866371.
[29] K.H. Hama Aziz, F.S. Mustafa, M.A.H. Karim, S. Hama, Pharmaceutical pollution in the aquatic environment: advanced oxidation processes as efficient treatment approaches: a review, Mater. Adv. 6 (2025) 3433–3454, https://doi.org/10.1039/d4ma01122h.
[30] M.A.H. Karim, K.H.H. Aziz, K.M. Omer, Y.M. Salih, F. Mustafa, K.O. Rahman, Y. Mohammad, Degradation of aqueous organic dye pollutants by heterogeneous photo-assisted Fenton-like process using natural mineral activator: parameter optimization and degradation kinetics, IOP Conf. Ser. Earth Environ. Sci. 958 (2022), https://doi.org/10.1088/1755-1315/958/1/012011.
[31] J. Wang, J.N. Park, H.C. Jeong, K.S. Choi, X.Y. Wei, S.I. Hong, C.W. Lee, Cu2+-exchanged zeolites as catalysts for phenol hydroxylation with hydrogen peroxide, Energy and Fuels 18 (2004) 470–476, https://doi.org/10.1021/ef0300904.
[32] K.M. Valkaj, V. Mandic, V.A. Katovic, Kataliticka oksidacija fenola uz zeolitni katalizator Cu/Y-5. 2. dio: utjecaj postsintetske termicke i kemijske obrade, Kem. u Ind. Chem. Chem. Eng. 64 (2015) 109–116, https://doi.org/10.15255/KUI.2013.033.
[33] E.G. Garrido-Ramírez, B.K.G. Theng, M.L. Mora, Clays and oxide minerals as catalysts and nanocatalysts in Fenton-like reactions - A review, Appl. Clay Sci. 47 (2010) 182–192, https://doi.org/10.1016/j.clay.2009.11.044.
[34] L. Amarasena, R. Weerasooriya, A. Bandara, L. Jayarathna, Exploring Depletion of Volatile Organic Compounds (VOCs) in the Air Using Faujasite zeolite Catalysts from Fundamental to Advanced, Springer International Publishing, 2024, https://doi.org/10.1007/s44292-024-00013-7.
[35] W.-C. Yang, Handbook of fluidization and fluid-particle systems, 2003. https://doi.org/10.1016/s1672-2515(07)60126-2.
[36] R. El Khawaja, S.K.P. Veerapandian, R. Bitar, N. De Geyter, R. Morent, N. Heymans, G. De Weireld, T. Barakat, Y. Ding, G. Abdallah, S. Sonar, A. Löfberg, J.-M. Giraudon, C. Poupin, R. Cousin, F. Cazier, D. Dewaele, P. Genevray, Y. Landkocz, C. Méausoone, N. Jaber, D. Courcot, S. Billet, J.-F. Lamonier, B.-L. Su, S. Siffert, Boosting VOCs elimination by coupling different techniques, Chem. Synth. 2 (2022) 13, https://doi.org/10.20517/cs.2022.10.
[37] T. Yin, X. Meng, L. Jin, C. Yang, N. Liu, L. Shi, Prepared hydrophobic Y zeolite for adsorbing toluene in humid environment, Microporous Mesoporous Mater 305 (2020) 110327, https://doi.org/10.1016/j.micromeso.2020.110327.
[38] R. Xu, W. Pang, J. Yu, Q. Huo, J. Chen, Chemistry of zeolites and related porous materials: synthesis and structure, 2010. https://doi.org/10.1002/9780470822371.
[39] M. Noorjahan, V. Durga Kumari, M. Subrahmanyam, L. Panda, Immobilized Fe(III)-HY: an efficient and stable photo-fenton catalyst, Appl. Catal. B Environ. 57 (2005) 291–298, https://doi.org/10.1016/j.apcatb.2004.11.006.
[40] S. Navalon, M. Alvaro, H. Garcia, Heterogeneous Fenton catalysts based on clays, silicas and zeolites, Appl. Catal. B Environ. 99 (2010) 1–26, https://doi.org/10.1016/j.apcatb.2010.07.006.

[41] H. Ayoub, T. Roques-carmes, O. Potier, B. Koubaissy, S. Pontvianne, Iron-impregnated zeolite catalyst for efficient removal of micropollutants at very low concentration from Meurthe river, (2018).
[42] L. Singh, P. Rekha, S. Chand, Cu-impregnated zeolite Y as highly active and stable heterogeneous fenton-like catalyst for degradation of Congo red dye, Sep. Purif. Technol. 170 (2016) 321–336, https://doi.org/10.1016/j.seppur.2016.06.059.
[43] E.V. Kuznetsova, E.N. Savinov, L.A. Vostrikova, V.N. Parmon, Heterogeneous catalysis in the Fenton-type system FeZSM-5/H 2O2, Appl. Catal. B Environ. 51 (2004) 165–170, https://doi.org/10.1016/j.apcatb.2004.03.002.
[44] X. Yang, X. Cheng, A.A. Elzatahry, J. Chen, A. Alghamdi, Y. Deng, Recyclable Fenton-like catalyst based on zeolite Y supported ultrafine, highly-dispersed Fe2O3 nanoparticles for removal of organics under mild conditions, Chinese Chem. Lett. 30 (2019) 324–330, https://doi.org/10.1016/j.cclet.2018.06.026.
[45] S. Hussain, E. Aneggi, D. Goi, Catalytic activity of metals in heterogeneous Fenton-like oxidation of wastewater contaminants: a review, Environ. Chem. Lett. 19 (2021) 2405–2424, https://doi.org/10.1007/s10311-021-01185-z.
[46] R. Mohite, A. Garg, Performance of supported copper catalysts for oxidative degradation of phenolics in aqueous medium: optimization of reaction conditions, kinetics, catalyst stability, characterization, and reusability, Ind. Eng. Chem. Res. 59 (2020) 12986–12998, https://doi.org/10.1021/acs.iecr.0c02211.
[47] H. Wang, R. Xu, Y. Jin, R. Zhang, Zeolite Structure Effects On Cu active center, SCR Performance and Stability of Cu-zeolite catalysts, Elsevier B.V., 2019, https://doi.org/10.1016/j.cattod.2018.04.035.
[48] K.M. Basha, A. Rajendran, V. Thangavelu, Recent advances in the biodegradation of phenol : a review, Asian J. Exp. Biol. Sci. 1 (2010) 219–234.
[49] R. Raja, P. Ratnasamy, Selective oxidation of phenols using copper complexes encapsulated in zeolites, Appl. Catal. A Gen. 143 (1996) 145–158, https://doi.org/10.1016/0926-860X(96)00077-4.
[50] E. Győri, Á. Kecskeméti, I. Fábián, M. Szarka, I. Lázár, Environment-friendly catalytic mineralization of phenol and chlorophenols with Cu- and Fe- tetrakis(4-aminophenyl)-porphyrin—Silica Hybrid aerogels, Gels 8 (2022) 202, https://doi.org/10.3390/gels8040202.
[51] C. Zhao, S. Zhong, C. Li, H. Zhou, S. Zhang, Property and mechanism of phenol degradation by biochar activated persulfate, J. Mater. Res. Technol. 9 (2020) 601–609, https://doi.org/10.1016/j.jmrt.2019.10.089.
[52] Y. Ghaffari, N.K. Gupta, J. Bae, K.S. Kim, Heterogeneous catalytic performance and stability of iron-loaded ZSM-5, zeolite-A, and silica for phenol degradation: a microscopic and spectroscopic approach, Catalysts 9 (2019), https://doi.org/10.3390/catal9100859.
[53] Y. Huang, X. Tian, Y. Nie, C. Yang, Y. Wang, Enhanced peroxymonosulfate activation for phenol degradation over MnO2 at pH 3.5–9.0 via Cu(II) substitution, J. Hazard. Mater. 360 (2018) 303–310, https://doi.org/10.1016/j.jhazmat.2018.08.028.
[54] J. Sun, G. Xia, W. Yang, Y. Hu, W. Shen, Microwave-assisted method to degrade phenol using persulfate or hydrogen peroxide catalyzed by Cu-bearing silicon carbide, Water Sci. Technol. (2020) 1–11, https://doi.org/10.2166/wst.2020.370.
[55] O. Chiyoda, M.E. Davis, Hydrothermal conversion of Y-zeolite using alkaline-earth cations, Microporous Mesoporous Mater 32 (1999) 257–264, https://doi.org/10.1016/S1387-1811(99)00112-2.
[56] B. Al-Zaidi, the Effect of Modification Techniques On the Performance of Zeolite-Y Catalysts in Hydrocarbon Cracking Reactions, The University of Manchester, 2011.
[57] Z. Liu, C. Shi, D. Wu, S. He, B. Ren, A simple method of preparation of high silica zeolite y and its performance in the catalytic cracking of cumene, J. Nanotechnol. 2016 (2016), https://doi.org/10.1155/2016/1486107.
[58] N. Taufiqurrahmi, A.R. Mohamed, S. Bhatia, Nanocrystalline zeolite Y: synthesis and characterization, IOP Conf. Ser. Mater. Sci. Eng. 17 (2011), https://doi.org/10.1088/1757-899X/17/1/012030.
[59] Z. Ayad, H.Q. Hussein, B.A. Al-Tabbakh, Synthesis and characterization of high silica HY zeolite by basicity reduction, in: AIP Conf. Proc., 2020, p. 2213, https://doi.org/10.1063/5.0000278.
[60] R.A. Rachman, U.T.I. Martia, W. Aulia, R.M. Iqbal, N. Widiastuti, F. Kurniawan, Combination of microbial fuel cell and zeolite Na-Y adsorption for chromium removal, in: AIP Conf. Proc., 2018, p. 2049, https://doi.org/10.1063/1.5082478.
[61] N. Taufiqurrahmi, A.R. Mohamed, S. Bhatia, Nanocrystalline Zeolite Y: synthesis and characterization, IOP Conf. Ser. Mater. Sci. Eng. 17 (2011) 012030, https://doi.org/10.1088/1757-899X/17/1/012030.
[62] L.B. Bortolatto, R.A.A. Boca Santa, J.C. Moreira, D.B. Machado, M.A.P.M. Martins, M.A. Fiori, N.C. Kuhnen, H.G. Riella, Synthesis and characterization of Y zeolites from alternative silicon and aluminium sources, Microporous Mesoporous Mater 248 (2017) 214–221, https://doi.org/10.1016/j.micromeso.2017.04.030.
[63] H. Li, R. Cheng, Z. Liu, C. Du, Waste control by waste: fenton–like oxidation of phenol over Cu modified ZSM–5 from coal gangue, Sci. Total Environ. 683 (2019) 638–647, https://doi.org/10.1016/j.scitotenv.2019.05.242.
[64] K.K. Bania, R.C. Deka, Zeolite-Y encapsulated metal picolinato complexes as catalyst for oxidation of phenol with hydrogen peroxide, J. Phys. Chem. C 117 (2013) 11663–11678, https://doi.org/10.1021/jp402439x.
[65] S. Chowdhury, K.G. Bhattacharyya, Use of Cu (II)- incorporated zeolite Y for decolourization of dyes in water : a case study with aqueous methylene blue and Congo red, SN Appl. Sci. 1 (2019) 1–9, https://doi.org/10.1007/s42452-018-0094-8.
[66] J.W. Ward, Spectroscopic study of the surface of zeolite Y. II. Infrared spectra of structural hydroxyl groups and adsorbed water on alkali, alkaline earth, and rare earth ion-exchanged zeolites, J. Phys. Chem. 72 (1968) 4211–4223, https://doi.org/10.1021/j100858a046.
[67] R. López-Fonseca, B. De Rivas, J.I. Gutiérrez-Ortiz, A. Aranzabal, J.R. González-Velasco, Enhanced activity of zeolites by chemical dealumination for chlorinated VOC abatement, Appl. Catal. B Environ. 41 (2003) 31–42, https://doi.org/10.1016/S0926-3373(02)00199-6.
[68] P.P. Knops-Gerrits, D.E. De Vos, E.J.P. Feijen, P.A. Jacobs, Raman spectroscopy on zeolites, Microporous Mater 8 (1997) 3–17, https://doi.org/10.1016/S0927-6513(96)00088-0.
[69] C. Brémard, M.Le Maire, Low-frequency Raman spectra of dehydrated faujasitic zeolites, J. Phys. Chem. 97 (1993) 9695–9702, https://doi.org/10.1021/j100140a028.
[70] D.M. Dal Pozzo, J.A. Azevedo Dos Santos, E.S. Júnior, R.F. Santos, A. Feiden, S. N. Melegari De Souza, I. Burgardt, Free fatty acids esterification catalyzed by acid faujasite type zeolite, RSC Adv 9 (2019) 4900–4907, https://doi.org/10.1039/c8ra10248a.
[71] K. Murakami, S. Fujioka, K. Mitani, M. Yamashita, M. Taguchi, Collection of simulated XRD powder patterns for zeolites, Kurinikaru Sutadi 4 (1983) 1063–1069. http://www.ncbi.nlm.nih.gov/pubmed/6557302.
[72] S.R. Batool, V.L. Sushkevich, J.A. van Bokhoven, Factors affecting the generation and catalytic activity of extra-framework aluminum lewis acid sites in aluminum-exchanged zeolites, ACS Catal. 14 (2024) 678–690, https://doi.org/10.1021/acscatal.3c04195.
[73] G. Li, C. Liu, R. Rohling, E.J.M. Hensen, E.A. Pidko, Lewis acid catalysis by zeolites. Model. Simul. Sci. Micro- Meso-Porous Mater., Elsevier, 2018, pp. 229–263, https://doi.org/10.1016/B978-0-12-805057-6.00007-7.
[74] S. Senthilkumar, W. Zhong, M. Natarajan, C. Lu, B. Xu, X. Liu, A green approach for aerobic oxidation of benzylic alcohols catalysed by CuI-Y zeolite/TEMPO in ethanol without additional additives, New J. Chem. 45 (2021) 705–713, https://doi.org/10.1039/d0nj03776a.
[75] Krylova Shelyapina, Zvereva Zhukov, Rodriguez-Iznaga, Fuentes-Moyado Petranovskii, Comprehensive analysis of the copper exchange implemented in ammonia and protonated forms of Mordenite using microwave and conventional methods, Molecules 24 (2019) 4216, https://doi.org/10.3390/molecules24234216.
[76] P. Vanelderen, J. Vancauwenbergh, B.F. Sels, R.A. Schoonheydt, Coordination chemistry and reactivity of copper in zeolites, Coord. Chem. Rev. 257 (2013) 483–494, https://doi.org/10.1016/j.ccr.2012.07.008.
[77] M.M. Lozinska, S. Jamieson, M.C. Verbraeken, D.N. Miller, B.E. Bode, C.A. Murray, S. Brandani, P.A. Wright, Cation ordering and exsolution in copper-containing forms of the flexible zeolite rho (Cu,M-Rho; M=H, Na) and their consequences for CO2 adsorption, Chem. - A Eur. J. 27 (2021) 13029–13039, https://doi.org/10.1002/chem.202101664.
[78] M.A. Oliver-Tolentino, A. Guzmán-Vargas, E.M. Arce-Estrada, D. Ramírez-Rosales, A. Manzo-Robledo, E. Lima, Understanding electrochemical stability of Cu+ on zeolite modified electrode with Cu-ZSM5, J. Electroanal. Chem. 692 (2013) 31–39, https://doi.org/10.1016/j.jelechem.2012.12.015.
[79] M.R. Abdi, H.R. Shakur, K.Rezaee Ebrahim Saraee, M. Sadeghi, Effective removal of uranium ions from drinking water using CuO/X zeolite based nanocomposites: effects of nano concentration and cation exchange, J. Radioanal. Nucl. Chem. 300 (2014) 1217–1225, https://doi.org/10.1007/s10967-014-3092-3.
[80] F. Sahraoui, N. Haddad, J.F. Lamonier, C. Rabia, Catalytic oxidation of volatile organic compounds alone or in mixture over Mg4Al2−xCex mixed oxides, Catalysts 13 (2023), https://doi.org/10.3390/catal13091269.
[81] D. Romero, D. Chlala, M. Labaki, S. Royer, J.P. Bellat, I. Bezverkhyy, J. M. Giraudon, J.F. Lamonier, Removal of toluene over naX zeolite exchanged with Cu2+, Catalysts 5 (2015) 1479–1497, https://doi.org/10.3390/catal5031479.
[82] B.Ba Mohammed, K. Yamni, N. Tijani, A.A. Alrashdi, H. Zouihri, Y. Dehmani, I. Chung, S. Kim, H. Lgaz, Adsorptive removal of phenol using faujasite-type Y zeolite: adsorption isotherms, kinetics and grand canonical Monte Carlo simulation studies, J. Mol. Liq. 296 (2019) 111997, https://doi.org/10.1016/j.molliq.2019.111997.
[83] M.A. Kuhn, Oxygen free radicals and antioxidants, Am. J. Nurs. 103 (2003) 58–62, https://doi.org/10.1097/00000446-200304000-00022.
[84] A. Plá-Hernández, F. Rey, A.E. Palomares, Pt-zeolites as active catalysts for the removal of chlorate in water by hydrogenation reactions, Catal. Today 429 (2024), https://doi.org/10.1016/j.cattod.2023.114461.
[85] S. Zrnčević, Z. Gomzi, CWPO: an environmental solution for pollutant removal from wastewater, Ind. Eng. Chem. Res. 44 (2005) 6110–6114, https://doi.org/10.1021/ie049182m.
[86] N. Chaouati, A. Soualah, M. Chater, Adsorption of phenol from aqueous solution onto zeolites y modified by silylation, Comptes Rendus. Chim. 16 (2013) 222–228, https://doi.org/10.1016/j.crci.2012.10.010.
[87] E.T. Saka, E. Dügdü, Y. Ünver, Degradation of substituted phenols with different oxygen sources catalyzed by Co(II) and Cu(II) phthalocyanine complexes, J. Coord. Chem. 72 (2019) 1119–1130, https://doi.org/10.1080/00958972.2019.1589461.
[88] A. Garg, A. Mishra, Degradation of organic pollutants by wet air oxidation using nonnoble metal-based catalysts, J. Hazardous, Toxic, Radioact. Waste 17 (2013) 89–96, https://doi.org/10.1061/(asce)hz.2153-5515.0000152.
[89] J. Al-Nu'Airat, B.Z. Dlugogorski, X. Gao, N. Zeinali, J. Skut, P.R. Westmoreland, I. Oluwoye, M. Altarawneh, Reaction of phenol with singlet oxygen, Phys. Chem. Chem. Phys. 21 (2019) 171–183, https://doi.org/10.1039/c8cp04852e.